

FE prediction of bearing capacity over reinforced soil

C.L. Nogueira

Department of Mines Engineering, School of Mine, UFOP, Ouro Preto/MG, Brazil

R.R.V. Oliveira & L.G. Araújo

Department of Civil Engineering, School of Mines, UFOP, Ouro Preto/MG, Brazil

P.O. Faria

Department of Civil Engineering - CTTMar – Univali, Itajaí/SC, Brazil

J.G. Zornberg

Department of Civil Engineering, University of Texas at Austin, Austin/TX, USA

ABSTRACT: This paper presents the numerical simulation using an elastoplastic analysis of the bearing capacity of shallow foundations. The problem involves axisymmetric conditions on reinforced soil using finite element method (FEM). The foundation soil is modeled as a non-associative elastoplastic Mohr-Coulomb material. The reinforcement is modeled as a linear elastic material. The ultimate bearing capacity obtained in this study is compared to solutions obtained using limit equilibrium and limit analysis. A parametric study was conducted for different configurations of reinforcement for a special case of frictionless foundation soil. The numerical results show good agreement with analytical results indicating the suitability of the numerical model used in this study and implemented into the code ANLOG - Non-Linear Analysis of Geotechnical Problems.

1 INTRODUCTION

An application of the finite element method (FEM) for non-linear elastoplastic analysis of reinforced soil structures under axisymmetric condition is presented in this paper.

The Mohr-Coulomb criterion suggested by Sloan & Booker (1986) and Abbo & Sloan (1995), which includes treatment of the singularities of the original Mohr-Coulomb criterion, is used for modeling the foundation soil. A general formulation that considers associative and non-associative elastoplastic models for soil was adopted. Hence, the influence of the dilatancy angle on the bearing capacity of reinforced soil could be investigated. The reinforcement is considered as linear elastic and the soil-reinforcement interface was considered rigid; thus interface elements were not considered in these analyses.

The numerical simulation was conducted using the code ANLOG – *Non Linear Analysis of Geotechnical Problems* (Zornberg, 1989; Nogueira, 1998; Pereira, 2003; Oliveira, 2006).

2 FINITE ELEMENT REPRESENTATION OF REINFORCED SOIL

A discrete representation for reinforced soil structures is adopted in this study. Each component of reinforced soil structure—the soil, the reinforcement and the soil-reinforcement interface—can be represented using a specific finite element with its own kinematic and constitutive equations. In the specific case of a bearing capacity problem of shallow foundations, the soil-reinforcement interface was considered rigid and therefore is not discussed in this paper.

In considering an incremental formulation by FEM, the kinematic equation that describes the relationship between the increment of strain ($\Delta\epsilon$) and the increment of nodal displacement ($\Delta\hat{u}$) in each finite element can be written as:

$$\Delta\epsilon = -B\Delta\hat{u} \quad (1)$$

where

$$\mathbf{B} = \nabla \mathbf{N} \quad (2)$$

∇ is a differential operator and \mathbf{N} is the matrix that contains the interpolation functions N_i . Both the operator and matrix depend on the type of element adopted. The negative sign in Equation 1 is a conventional indicator of positive compression.

The increment of stress ($\Delta \boldsymbol{\sigma}$) can be obtained using the incremental constitutive equation:

$$\Delta \boldsymbol{\sigma} = \mathbf{D}_t \Delta \boldsymbol{\epsilon} \quad (3)$$

where \mathbf{D}_t is the constitutive matrix defined in terms of the elastoplasticity formulation as:

$$\mathbf{D}_t = \mathbf{D}_e - \mathbf{D}_p \quad (4)$$

where \mathbf{D}_e is the elastic matrix and \mathbf{D}_p is the plastic parcel of the constitutive matrix defined as:

$$\mathbf{D}_p = \frac{\mathbf{D}_e \mathbf{b} (\mathbf{D}_e \mathbf{a})^T}{\mathbf{a}^T \mathbf{D}_e \mathbf{b} + H} \quad (5)$$

\mathbf{a} is the gradient of the yield function ($F(\boldsymbol{\sigma}, h)$), \mathbf{b} is the gradient of the potential plastic function ($G(\boldsymbol{\sigma}, h)$), h is the hardening parameter and H is the hardening modulus. In the case of perfect plasticity, since hardening is not considered, H equals zero.

Starting from an equilibrium configuration where the displacement field, the strain state, and the stress state are all known, a new equilibrium configuration, in terms of displacements, can be obtained using the modified Newton Raphson procedure with automatic load increment (Nogueira, 1998). In this paper, only the elastic parcel of the constitutive matrix was considered in the iterative procedure used to obtain the global stiffness matrix.

At each increment the iterative scheme satisfies, for a selected tolerance, the global equilibrium, compatibility conditions, boundary conditions and constitutive relationships. Yet attention must be given to the stress integration scheme adopted to obtain the stress increments (Equation 3), in order to guarantee the Kuhn-Tucker conditions and the consistency condition.

2.1 Soil representation

The soil is represented by the quadratic quadrilateral isoparametric element (Q8). This element has two degree of freedom, u and v , in the directions r and y (radial and axial), respectively. The stress and strain vectors are defined as:

$$\boldsymbol{\sigma}^T = [\sigma_r \quad \sigma_y \quad \sigma_\theta \quad \tau_{ry}] \quad (6)$$

$$\boldsymbol{\epsilon}^T = [\epsilon_r \quad \epsilon_y \quad \epsilon_\theta \quad \gamma_{ry}] \quad (7)$$

In which $\epsilon_\theta = u/r$. The kinematic matrix \mathbf{B} can be written as:

$$\mathbf{B} = \begin{bmatrix} \partial N_1 / \partial r & 0 & \partial N_8 / \partial r & 0 \\ 0 & \partial N_1 / \partial y & 0 & \partial N_8 / \partial y \\ N_1 / r & 0 & N_8 / r & 0 \\ \partial N_1 / \partial y & \partial N_1 / \partial r & \partial N_8 / \partial y & \partial N_8 / \partial r \end{bmatrix} \quad (8)$$

where N_i is the i node shape function by the finite element Q8 (Nogueira, 1998). The stiffness matrix for axisymmetric condition for this element is given by:

$$\mathbf{K} = \int_{-1}^{-1} \int_{-1}^{+1} [\mathbf{B}^T \mathbf{D}_t \mathbf{B} (2\pi (\mathbf{N} \hat{\mathbf{r}}) \det \mathbf{J})] d\xi d\eta \quad (9)$$

where $\hat{\mathbf{r}}$ is the nodal global coordinate vector; (ξ, η) is the natural coordinate system and \mathbf{J} is the Jacobian operator.

To describe the stress-strain relationship a perfectly elastoplastic model with non-associative plasticity was adopted. The plastic parcel of the constitutive matrix is obtained using the modified Mohr-Coulomb criterion proposed by Sloan & Booker (1986) and Abbo & Sloan (1995) (Figure 1). The modified version of the Mohr-Coulomb model involves removal of the singularities at the edges ($\theta = \pm\pi/6$) and the apex of the original model. Its yield function is written as:

$$F = \sqrt{I_{2D}(K(\theta))^2 + (a \sin \phi)^2} - (I_1/3) \sin \phi - c \cos \phi \quad (10)$$

where

$$\theta = (1/3) \sin^{-1} \left((-1.5\sqrt{3}) I_{3D} (I_{2D})^{-3/2} \right) \quad \theta \in [-\pi/6; \pi/6] \quad (11)$$

θ is the Lode angle, I_1 is the first invariant of the stress tensor; I_{2D} is the second invariant of the deviator stress tensor, I_{3D} is the third invariant of the deviator stress tensor, c and ϕ are the material cohesion and internal friction angle, respectively. A transition angle (θ_T) was introduced to define the $K(\theta)$ function on the Equation 10. Sloan & Booker (1986) suggest θ_T value range from 25° to 29° . For the case in which $|\theta| > \theta_T$,

$$K(\theta) = A + B \sin 3\theta \quad (12)$$

where

$$A = (1/3) \cos \theta_T \left(3 + \tan \theta_T \tan 3\theta_T + (1/\sqrt{3}) \text{signal}(\theta) (3 \tan \theta_T - \tan 3\theta_T) \sin \phi \right) \quad (13)$$

$$B = (1/(3 \cos 3\theta_T)) \left(\text{signal}(\theta) \sin \theta_T - (1/\sqrt{3}) \cos \theta_T \sin \phi \right) \quad (14)$$

Or, for the case in which $|\theta| \leq \theta_T$

$$K(\theta) = \cos \theta + \frac{1}{\sqrt{3}} \sin \theta \sin \phi \quad (15)$$

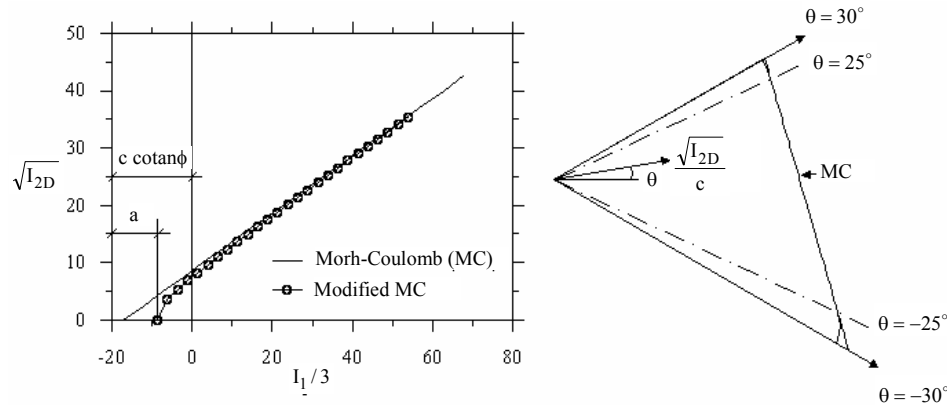


Figure 1 - Mohr-Coulomb yield function (Abbo & Sloan, 1995).

The parcel $a \sin \phi$ was introduced to prevent the singularity related to the surface apex. For the parameter “a” Abbo & Sloan (1995) recommend 5% of $(c \cotan \phi)$. The potential plastic function (G) can be written the same way as the yield function (F) but using the dilatancy angle (ψ) instead of the friction angle (ϕ).

An important step in a non linear analysis using MEF relates to the integration of the constitutive equation. This equation defines a set of ordinary differential equations for which the integration methodology can be either implicit or explicit. In this paper an explicit process with sub incrementation, as proposed by Sloan et al. (2001), was adopted. This methodology uses the modified Euler scheme that determines the size of the sub increment automatically evaluating the local error induced during integration of the parcel stress plastic.

2.2 Reinforcement representation

The reinforcement is represented by quadratic one-dimensional isoparametric elements (R3) (Oliveira, 2006). The reinforcement thickness is considered in the constitutive equation. This element has one degree of freedom, u' , on its own longitudinal direction r' . The longitudinal direction is related to the radial direction on the local coordinate system according to the following transformation:

$$\mathbf{r}' = \mathbf{N}\mathbf{T}\hat{\mathbf{r}} \quad (16)$$

In which \mathbf{N} is the matrix that contains the shape functions (N_i) for this element (Oliveira, 2006), $\hat{\mathbf{r}}^T = [r_1 \quad y_1 \quad \cdots \quad r_3 \quad y_3]$ is the nodal global coordinate vector, and

$$\mathbf{T} = \begin{bmatrix} \cos\beta & \sin\beta & \cdots & \cdots & 0 & 0 \\ \vdots & \vdots & \vdots & \vdots & \vdots & \vdots \\ 0 & 0 & \cdots & \cdots & \cos\beta & \sin\beta \end{bmatrix} \quad (17)$$

where $\cos\beta = (dr/d\xi)/\det\mathbf{J}$; $\sin\beta = (dy/d\xi)/\det\mathbf{J}$; $\det\mathbf{J} = \sqrt{(dr/d\xi)^2 + (dy/d\xi)^2}$; $\frac{dr}{d\xi} = \sum_{i=1}^3 \left(\frac{dN_i}{d\xi} r_i \right)$

and $\frac{dy}{d\xi} = \sum_{i=1}^3 \left(\frac{dN_i}{d\xi} y_i \right)$.

The R3 element has two components of strain and stress: longitudinal ($\varepsilon_{r'}$ and $\sigma_{r'}$) and circumferential ($\varepsilon_{\theta'}$ and $\sigma_{\theta'}$). The kinematic condition is given by the relation:

$$\boldsymbol{\varepsilon}' = -\mathbf{B}\hat{\mathbf{u}}' = - \begin{bmatrix} \frac{1}{\det\mathbf{J}} \frac{\partial N_1}{\partial \xi} & \cdots & \frac{1}{\det\mathbf{J}} \frac{\partial N_3}{\partial \xi} \\ \frac{N_1}{r'} & \cdots & \frac{N_3}{r'} \end{bmatrix} \mathbf{T}\hat{\mathbf{u}} \quad (18)$$

where $\hat{\mathbf{u}}$ is the vector of the nodal global displacement components (u, v).

The constitutive matrix for the reinforcement element is given by:

$$\mathbf{D}_t = \left(\frac{J/t}{1-v^2} \right) \begin{bmatrix} 1 & v \\ v & 1 \end{bmatrix} \quad (19)$$

where J is the reinforcement stiffness (kN/m), t is the reinforcement thickness and v is the Poisson ratio.

The reinforcement stiffness matrix under axisymmetric condition is given by:

$$\mathbf{K} = \int_{-1}^{+1} \left[(\mathbf{B}\mathbf{T})^T \mathbf{D}_t (\mathbf{B}\mathbf{T}) (2\pi t (\mathbf{N}\hat{\mathbf{r}}) \det\mathbf{J}) \right] d\xi \quad (20)$$

3 BEARING CAPACITY ON UNREINFORCED SOIL

The analyses presented in this study involve smooth circular foundation subjected to vertical loading acting on the ground surface. The problem is analyzed under axisymmetric condition and is modeled as both flexible and rigid foundation using load and displacement controls respectively (Figure 2). The foundation soil is considered weightless. As mentioned the soil is considered as an elastic perfectly plastic material described by a non-associative modified Mohr-Coulomb model. Both the friction and dilatancy angle were varied to assess their influence on the bearing capacity of the shallow foundation. According to Houlsby (1991) the dilatancy is a key factor in geotechnical problems involving kinematic movement restrictions, such as the bearing capacity of shallow and deep foundations. Results of this study are compared with results of studies that utilize equilibrium limit and limit analysis theories.

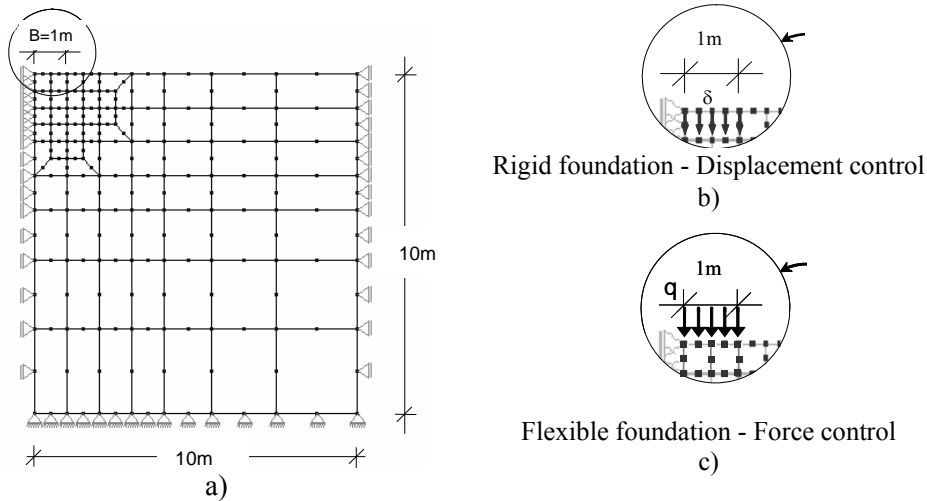


Figure 2 - Finite element mesh: a) full mesh; b) detail of the displacement imposed boundary condition; c) detail of stress imposed boundary condition

An incremental-iterative modified Newton Raphson scheme with automatic loading increments is used considering a tolerance of 10^{-4} for the force criterion of convergence. For the stress integration algorithm the following tolerances are used: FTOL= 10^{-9} and STOL= 10^{-8} . The FTOL tolerance is related to the transition condition from elastic to plastic state which is affected by the finite precision arithmetic. The STOL tolerance is related to the local error in the stresses in the Euler modified schemes.

Numerical results are presented in terms of the κ factor which is a normalized stress defined as:

$$\kappa = Q / (Ac) = q / c \quad (21)$$

in which A is the footing area and Q is the reaction force at the foundation, defined as:

$$Q = \sum_{e=1}^n \left(\int_{V_e} \mathbf{B}^T \boldsymbol{\sigma}_e dV_e \right) \quad (22)$$

The reaction force is evaluated as the sum of the internal force's vertical components equivalent to the elements's stress state right beneath the foundation. The cohesion is adopted to normalize the results but in the case of cohesionless soil the atmospheric pressure can be adopted instead.

Figure 3 presents the κ factor versus normalized settlement (δ/B) curves obtained by ANLOG for flexible and rigid foundations and for different values of friction and dilatancy angles. It can be observed that associative analysis ($\psi=\phi$) provides the lowest displacement at failure.

Table 1 presents normalized ultimate bearing capacity (κ_{ult}), as shown in Figure 3. As expected, the κ_{ult} value obtained for rigid foundation is higher than that obtained for a flexible foundation. The difference in κ_{ult} values was approximately 9.5%, but the highest difference was observed in non-associative plasticity (approximately 11.2%).

Analyses conducted in this study show that when the friction angle was decreased to 10° and 20° , the ultimate bearing capacity factor (κ_{ult}) was no longer affected by the dilatancy angle. For friction angle of 30° the associate plasticity analysis ($\psi=\phi$) provided the highest ultimate bearing capacity factor and the lowest displacement at failure. Zienkiewicz et al. (1975) observed a similar response for friction angles of 40° . Monahan & Dasgupta (1993) reported such behavior for friction angles higher than 25° .

Table 2 presents a comparison between results obtained using ANLOG and those from a classical solution from equilibrium limit by Terzaghi (1943), limit analyses solution by Chen

(1975), and a recent numerical solution based on limit analyses using FEM by Ribeiro (2005). Good agreement can be observed among these results.

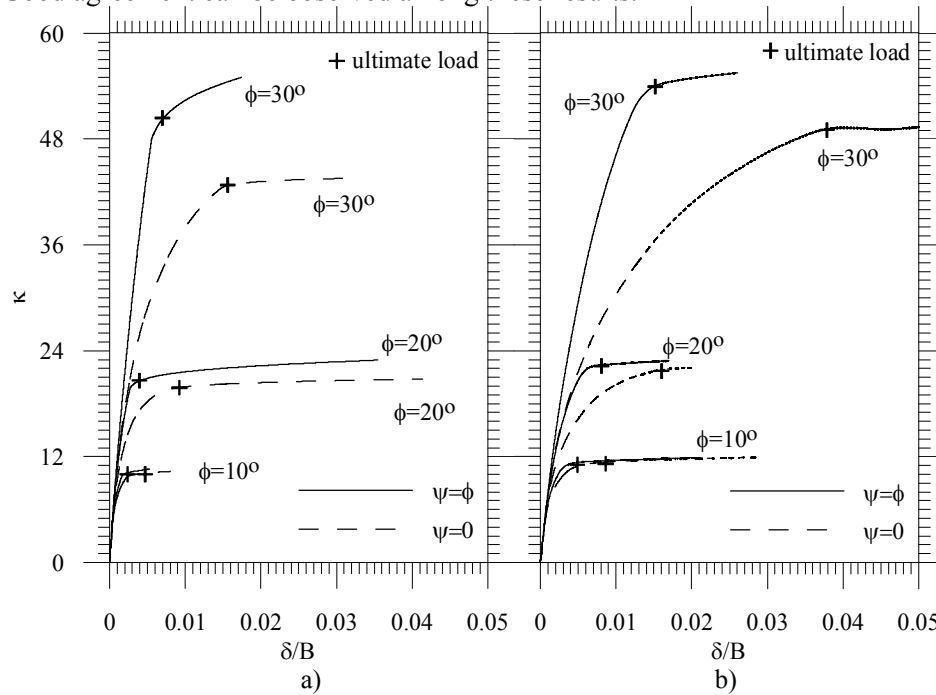


Figure 3 - Load versus displacement curves: a) Flexible foundation; b) Rigid foundation

Table 1 - Normalized ultimate bearing capacity ($\kappa_{ult} = q_{ult} / c$)

$\phi(^{\circ})$	$\Psi(^{\circ})$	Flexible Foundation	Rigid Foundation
10	0	10.1	11.4
	10	10.4	11.4
20	0	20.0	22.0
	20	20.4	22.4
30	0	43.4	49.5
	30	49.5	54.0

Table 2 - Ultimate bearing capacity values for flexible circular footing and associative plasticity

$\phi(^{\circ})$	This study κ_{ult}	Terzaghi (1943) ($1.3N_c$)	Chen (1975)	Ribeiro (2005)
10	10.4	10.86	9.98	11.91
20	20.4	19.29	20.1	24.87
30	49.5	39.18	49.3	52.76

4 BEARING CAPACITY ON REINFORCED SOIL

A rigid rough circular shallow foundation subjected to vertical loading is analyzed using different reinforcement configurations. The soil is considered frictionless, weightless and elastic perfectly plastic with the following properties: $E=10\text{MPa}$; $\nu=0.49$, $c=30\text{kPa}$, $\phi=0^{\circ}$, $a=0$, $\theta_1=28^{\circ}$. The dilatancy angle (ψ) was varied during the study. A reinforcement of 4 m in diameter is considered linear elastic with: $t=2.5\text{mm}$, $J=2500\text{ kN/m}$ and $\nu=0$. The interface soil-reinforcement was considered rigid and therefore interface elements are not considered in these analyses. The finite element mesh and the boundary conditions are presented in Figure 4.

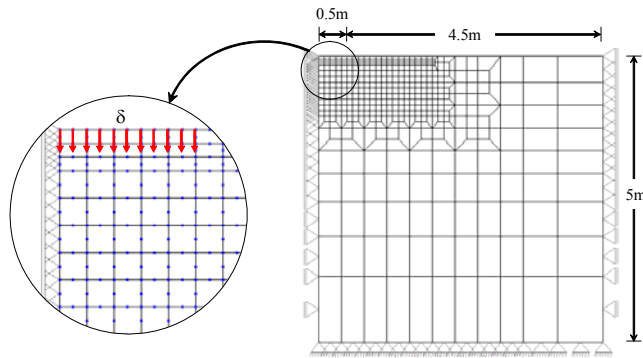


Figure 4 - Finite element mesh – Rigid rough circular without embedment shallow foundation

Figure 5 illustrates the reinforcement layout considered in this study. B is the circular footing diameter, U is the depth to the first reinforcement layer, H is the space between each reinforcement layer, N is the number of reinforcement layers; b is the diameter of reinforced zone and d is the depth of the last reinforcement layer.

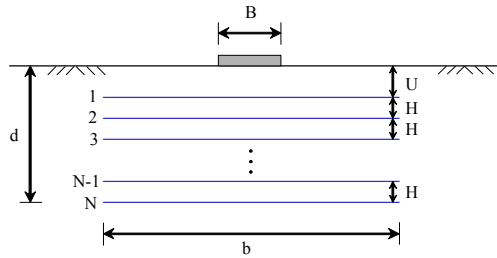


Figure 5 - Layout of the rigid foundation on reinforced soil

4.1 Unreinforced foundation

For an unreinforced foundation, the κ_{ult} value obtained by ANLOG was 5.42. Potts and Zdravković (2001) have obtained 5.39. The difference, approximately 0.5%, is considered negligible. At this level the settlement obtained by ANLOG was 0.025m.

Figure 6 illustrates the failure mechanism with displacement vectors. The failure mechanism is consistent with that proposed by Prandtl (1920) for strip footing.

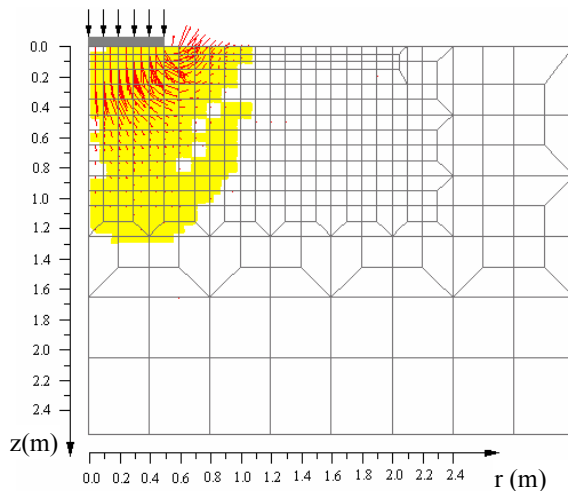


Figure 6 - Failure mechanism – unreinforced soil

4.1 Reinforced foundation

Prediction of the bearing capacity was initially conducted considering a single layer of reinforcement under axisymmetric condition. The diameter of the reinforced zone is constant ($b=4B$) while the reinforcement depth varies from $0.05 B$ to $0.9 B$.

The bearing capacity improvement is evaluated by quantifying the bearing capacity ratio (BCR) defined as:

$$BCR = \frac{\kappa}{\kappa_{ult}^0} \quad (23)$$

in terms of the κ factor for the reinforced soil foundation and the ultimate bearing capacity for the unreinforced soil foundation (κ_{ult}^0). For consistency, the BCR must be evaluated at a particular settlement level. For instance, $BCR_{0.1}$ means the bearing capacity improvement is being evaluated with the κ factor at a normalized settlement (δ/B) of 0.1.

The settlement reduction improvement is evaluated by the settlement reduction ratio (SRR) which is defined as:

$$SRR(\%) = \left[\frac{\delta^0 - \delta^r}{\delta^0} \right] 100 \quad (24)$$

where δ^0 is the settlement at the ultimate load of unreinforced foundation soil and δ^r is the settlement of reinforced foundation soil at the ultimate load of unreinforced soil foundation. Figure 7 illustrates these indexes.

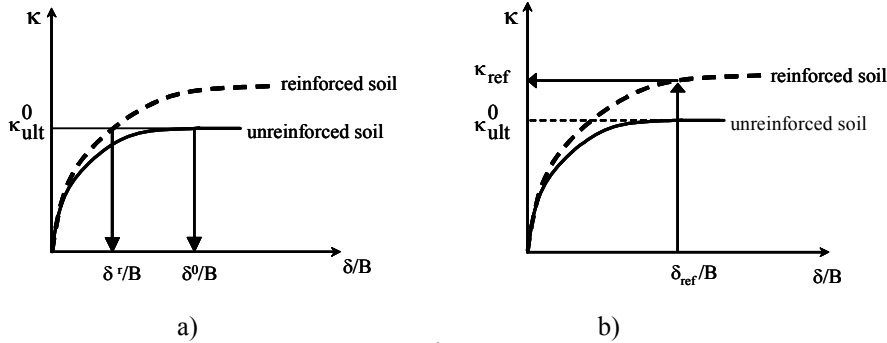


Figure 7 - References parameters: a) δ^r/B definition; b) κ_{ref} definition

As expected, the settlement decreases because of the reinforcement of the foundation soil. A region can be defined through where the reinforcement location maximizes the SRR. In this case the higher value of SRR was around 40% from $0.05B$ to $0.35B$ (Figure 8). In terms of bearing capacity improvement, the results provided in Figure 8 indicate that there is little improvement for a single layer of reinforcement (maximum BCR was 14%). It should also be noted that there is an optimum depth as well as a limit depth, beyond which no improvement is verified.

Figure 9 presents the displacement field at the failure for unreinforced soil foundation and the optimum and limit reinforcement positions. Note that the limit depth (U_{limit}) coincides with the lowest point of the failure wedge and the optimum depth ($U_{optimum}$) coincides with a high level of mobilized shear stress for the unreinforced foundation soil.

The numerical results suggest that the reinforcement starts to work after the soil deforms plastically. To investigate the influence of the number of reinforcement layers, the foundation settlement reference of $0.05 m$ is adopted. Although this value is high in terms of allowed settlement for a shallow foundation it was adopted to ensure that the load in the reinforcement is mobilized. The baseline geometry was: $B=1m$, $U/B=0.05$, $H/B=0.1$ and $b/B=4$. The parametric evaluation involved varying the number of the reinforcement layers (N). Results are shown in Figure 10.

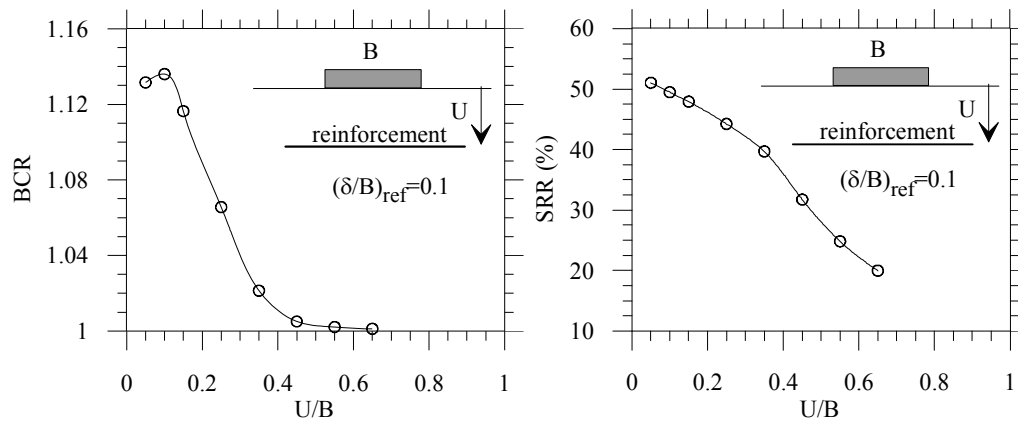


Figure 8 - U/B influence on the BCR and the SRR

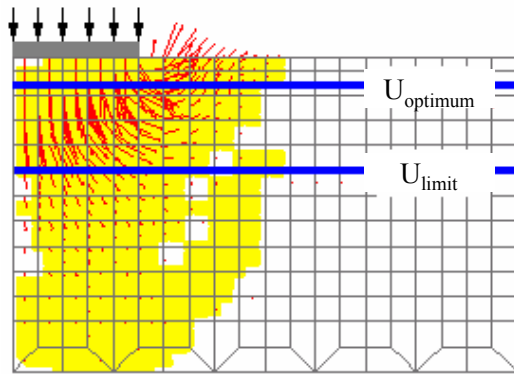


Figure 9 - Optimum and limit reinforcement position

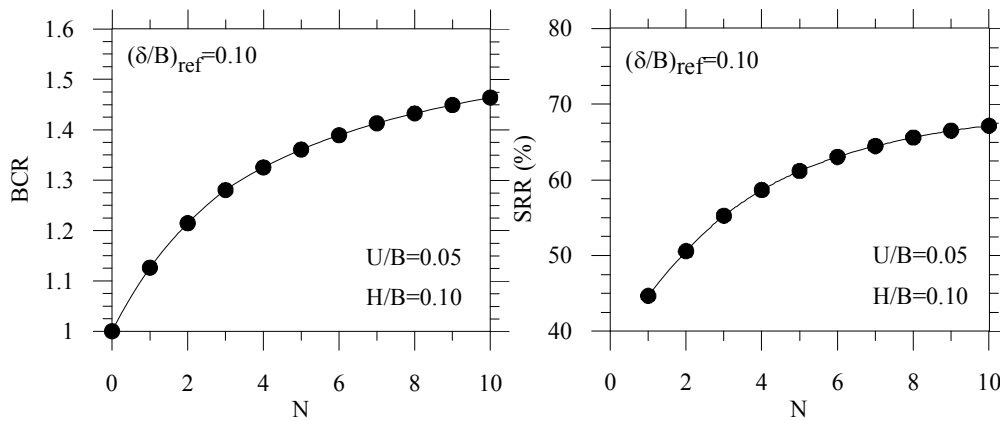


Figure 10 - Influence of the number of reinforcement layers

In this case, which involved circular footing and frictionless soil foundation, the bearing capacity improvement (BCR) was around 10% and the settlement reduction ratio (SRR) was around 6% as the number of reinforcements was increased from 5 to 10. Accordingly, the number of reinforcement layers should not exceed 4 to 7.

A second parametric evaluation involved assessment of the influence of the space between each reinforcement layer (H) varying the number of reinforcement layers from 2 to 5. The geometry was: $B=1\text{m}$, $U/B=0.05$ and $b/B=4$. Figure 11 presents the bearing capacity ratio (BCR) in terms of the number of reinforcement layers (N). Two different spaces between the reinforcement layers are considered: $H/B=0.10$ and 0.20 . It can be observed that the bearing capacity increases as the spacing decreases.

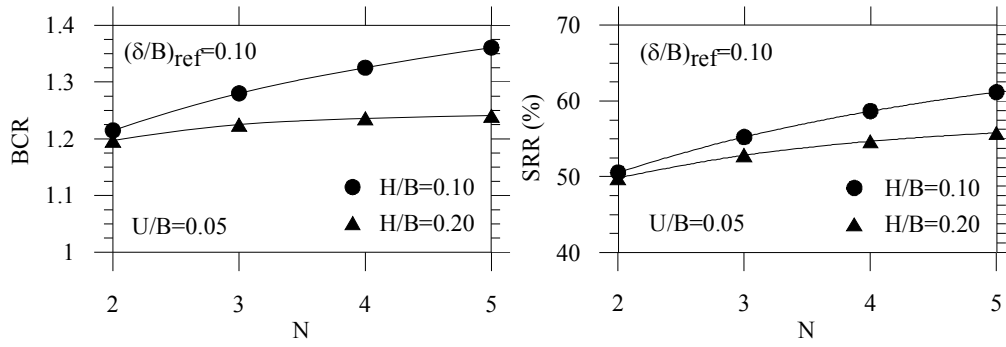


Figure 11 - Influence of the space between each reinforcement layer

Figure 12 shows the horizontal displacement field of the unreinforced soil and of two configurations of reinforced soil ($H/B=0.10$ and $H/B=0.20$). This displacement field is at the settlement level corresponding to an ultimate level of unreinforced soil ($\delta/B=0.05$). The number of reinforcement layers ($N=5$) and the position of the first reinforcement layer ($U/B=0.05$) are constant. The lowest horizontal displacement was observed when the H/B is 0.10. As expected, the results confirmed that high confinement improves bearing capacity.

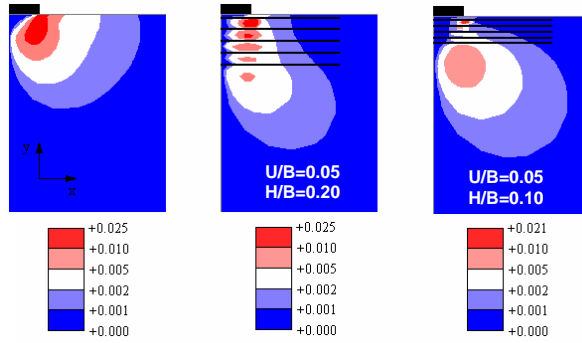


Figure 12 - Horizontal displacement (m) – rigid foundation ($\delta_{ref}/B=0.1$)

Adopting the foundation settlement reference (δ_{ref}) of 0.05 m and maintaining $B=1m$, $H/B=0.1$, $N=5$ and $b/B=4$ as constant, the influence of the depth of the first reinforcement layer (U) was analyzed. In order to explain this influence the curve BCR versus U/B (Figure 13) was divided into 3 zones in terms of the bounded values $(U/B)_{optimum}$ and $(U/B)_{limit}$. Zone 1 defines the suitable values for the position of the first layer. Zone 2 is characterized by a significant decrease in the bearing capacity ratio. In Zone 3 shows no improvement in bearing capacity. In this case the bounded values, $(U/B)_{optimum}$ and $(U/B)_{limit}$, was respectively around 0.05 and 0.25.

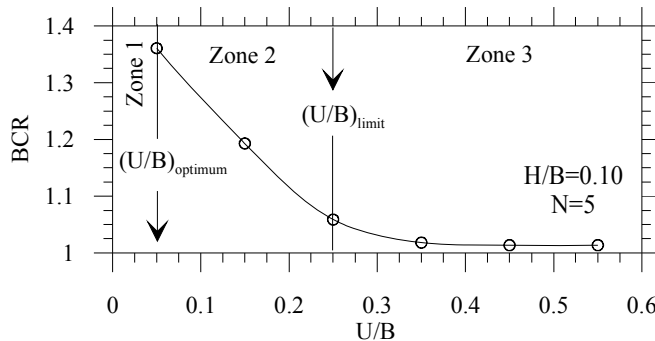


Figure 13 - Influence of the first reinforcement layer depth – ($\delta_{ref}/B=0.1$)

Figure 14 shows the failure mechanisms for the case in which the depth of the top reinforcement layer exceeds $(U/B)_{\text{limit}}$. Note that the reinforced layer of soil works as a rigid and rough base. In this region both vertical and horizontal displacements are approximately zero.

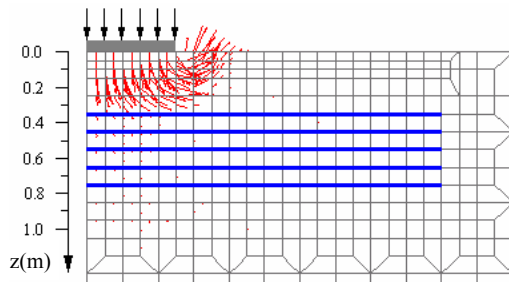


Figure 14 - Influence of the first reinforcement layer depth – ($\delta_{\text{ref}}/B=0.1$)

5 CONCLUSIONS

This paper presented a numerical simulation using FEM to analyze the bearing capacity of shallow foundations on reinforced soil under axisymmetric conditions. The modified Mohr-Coulomb constitutive model was implemented into ANLOG. The implementation of the explicit integration stress algorithm proposed by Sloan et al (2001) was needed in order to obtain good performance of the Newton Raphson algorithm at the global level.

The numerical results confirmed that the ultimate bearing capacity of a rigid shallow foundation on unreinforced soil is higher than that on a flexible shallow foundation. The ultimate bearing capacity of flexible foundations obtained numerically shows good agreement with the results obtained by equilibrium limit theory (Terzaghi, 1943) and limit analysis (Chen, 1975; Ribeiro, 2005).

The ultimate bearing capacity of unreinforced soil was not affected by the dilatancy angle when the friction angle is low but is relevant for comparatively high friction angles. Therefore, for a high friction angle the κ_{ult} values are a little high in the case of associative plasticity. In general, the non-associative plasticity provides higher settlement at failure. Results presented in this paper agree with the results provided by Monahan & Dasgupta (1995) and Zienkiewics et al (1975).

In order to show the influence of the reinforcement on the bearing capacity and settlement reduction, a parametric study was conducted using different reinforcement configurations. A rigid, rough, and shallow foundation under axisymmetric condition was considered in the analysis. The soil foundation was considered weightless and purely cohesive ($\phi=0^\circ$) and the interface soil-reinforcement was considered rigid. Based on the results, it may be concluded that:

The bearing capacity increases and the settlement reduction increases as the number of reinforcement layers increase. A cost-benefit analysis should be conducted to define the optimum number of reinforcement layers to be used.

The bearing capacity ratio, which indicates the improvement on the bearing capacity, was approximately 14% for just one reinforcement layer; it may be considered modest. In this case the optimum depth for placing it is $0.1B$ and the limit depth is $0.5B$. The reinforcement influence on the settlement, however, is significant (around 40% to 50%). The reinforcement starts to work after the soil deforms plastically, which often occur at a high level of settlement.

The results show the existence of three regions related to the depth of the first reinforcement layer to consider. The first, Zone 1, defines the suitable value for this depth. Zone 2 is characterized by a significant decrease in the bearing capacity ratio. Zone 3 corresponds to a lack of no influence on the bearing capacity. Effort should be made to identify these zones in order to define the best position for the reinforcement layer.

ACKNOWLEDGMENTS

The authors are grateful for the financial supports received by the first author from CAPES (Coordinating Agency for Advanced Training of High-Level Personnel – Brazil) and by the second author from Maccaferri do Brasil LTDA. They also acknowledge the Prof. John Whites for the English revision of this text.

REFERENCES

- Abbo, A.J. & Sloan, S.W. 1995. A smooth hyperbolic approximation to the Mohr-Coulomb yield criterion. *Computers & Structures*, 54(3): 427-441.
- Chen, W.F. 1975. *Limit Analysis and Soil Plasticity*. Elsevier Science Publishers, BV, Amsterdam, The Netherlands.
- Houlsby, G.T. 1991. How the dilatancy of soils affects their behaviour, *Proc. X Euro. Conf. Soil Mech. Found. Engng.*, Firenze 1991, (4):1189-1202.
- Manohan, N. & Dasgupta, S.P. 1995. Bearing capacity of surface footings by finite element. *Computers & Structures*, (4): 563-586.
- Nogueira, C.L. 1998. Non-linear analysis of excavation and fill. *DS. Thesis*. PUC/Rio, RJ, 265p (in Portuguese).
- Oliveira, R.R.V. 2006. Elastoplastic analysis of reinforced soil structures by FEM. *MS. Thesis*. PROPEC/UFOP (in Portuguese).
- Pereira, A.R. 2003. Physical non-linear analysis of reinforced soil structures. *MS. Thesis*. PROPEC/UFOP (in Portuguese).
- Potts, D.M. & Zdravković, L. 2001. *Finite Element analysis in geotechnical engineering: application*. Thomas Telford Ltda.
- Ribeiro, W.N. 2005. Applications of the numerical limit analysis for axisymmetric stability problems in Geotechnical Engineering. *MS. Thesis*, UFOP (in Portuguese).
- Sloan, S.W. & Booker, J.R. 1986. Removal of singularities in Tresca and Mohr-Coulomb yield criteria, *Communications in Applied Numerical Methods*, (2): 173-179.
- Sloan, S.W.; Abbo, A.J. & Sheng, D. 2001. Refined explicit integration of elastoplastic models with automatic error control, *Engineering Computations*, 18(1): 121-154.
- Terzaghi, K. 1943. *Theoretical Soil Mechanics*. Wiley.
- Zienkiewicz, O.C., Humpheson, C. & Lewis, R.W. 1975. Associated and non-associated visco-plasticity and plasticity in soil mechanics. *Geotechnique*, 25(4): 671-689.
- Zornberg, J.G. 1989. Finite element analysis of excavations using an elasto-plastic model. *MS. Thesis*. PUC-Rio, Rio de Janeiro (in Portuguese).